The density of states and the electron concentration of a double-heterojunction system subjected to an in-plane magnetic field

1999 J. Phys.: Condens. Matter 11 5131

(http://iopscience.iop.org/0953-8984/11/26/314)

J. Phys.: Condens. Matter **11** (1999) 5131–5141. Printed in the UK PII: S0953-8984(99)02270-5

The density of states and the electron concentration of a double-heterojunction system subjected to an in-plane magnetic field

C D Simserides

INFM and Scuola Normale Superiore, Piazza dei Cavalieri 7, I-56126 Pisa, Italy

Received 1 March 1999

Abstract. We calculate the electronic states of $Al_xGa_{1-x}As/GaAs/Al_xGa_{1-x}As$ double heterojunctions subjected to a magnetic field parallel to the quasi-two-dimensional electron gas layer. We study the energy dispersion curves, the density of states, the electron concentration and the distribution of the electrons in the subbands.

The parallel magnetic field induces severe changes in the density of states, which are of crucial importance for the explanation of the magnetoconductivity in these structures. However, to our knowledge, there has been no systematic study of the density of states under these circumstances. We attempt a contribution in this direction.

For symmetric heterostructures, the depopulation of the higher subbands, the transition from a single-layer to a bilayer electron system and the domination of the bulk Landau levels in the centre of the wide quantum well, as the magnetic field is continuously increased, are presented in the 'energy dispersion picture' as well as in the 'electron concentration picture' and in the 'density-of-states picture'.

1. Introduction

Although the behaviour of the quasi-two-dimensional electron gas (Q2DEG) in the presence of a perpendicular magnetic field has been studied extensively, much less attention has been devoted to the situation where the magnetic field is applied parallel to the Q2DEG layer. In the former case, interesting phenomena, e.g. the Shubnikov–de Haas effect [1] and the integer [2] and the fractional [3] quantum Hall effects, have been observed. In the latter case, electrons move under the competing influence of the Lorentz force and the force due to the quantum well confining potential.

In the presence of an in-plane magnetic field, $\vec{B}$, single heterojunctions [4–6], single [7, 8], double [8–12] and triple [13] square quantum wells, almost square quantum wells [14, 15], asymmetric square quantum wells [16], symmetrical wide single quantum wells [17, 18] and superlattices [19] have been considered.

The experimental studies include ones of single heterojunctions [6], double square quantum wells [10–12], triple square quantum wells [13], wide single quantum wells [18] and superlattices [19]. The most important experimental finding [10, 12, 13, 18] is, in our opinion, the strong conductance 'oscillations' due to the variation of the density of states (DOS), as B is increased. Conductance maxima are identified with depopulations of local energy dispersion minima, while conductance minima are identified with van Hove singularities at the chemical potential. This situation has been encountered for symmetrical square double [10, 12] and

0953-8984/99/265131+11$19.50

triple [13] quantum wells and for symmetrical wide single quantum wells [18]. While in the cases of square double and triple quantum wells a simple tight-binding calculation gave the position of the maxima and the minima, a self-consistent calculation was necessary in the case of symmetrical wide single quantum wells.

Theoretical studies of the electronic states are usually restricted to simple analytically solvable potential wells, to tight-binding approximation, or to perturbative approximations. Self-consistent studies have been few, and they have focused on single heterojunctions [4, 5], thin single quantum wells [14] and symmetrical wide single quantum wells [17].

In the present work, we study the $Al_xGa_{1-x}As/GaAs/Al_xGa_{1-x}As$ wide double heterojunction (i.e. a system of two heterojunctions with a relatively large distance between the two interfaces) subjected to an in-plane magnetic field using self-consistent calculations. Below, we summarize the particular aims of this work.

Our first aim is to study the density of states when the Q2DEG is subjected to an in-plane magnetic field. In this case, the DOS is not a step-like function, as it is with $B = 0$. We show that its form undergoes important changes as B is increased, especially in wide double heterojunctions where usually many subbands are present [20, 21]. The self-consistent study of the electronic states and specifically of the DOS is of great importance for the explanation of the experimental magnetoconductivity in these structures. However, up to now, there has been no systematic study of the DOS under these circumstances. We attempt to give a contribution in this direction.

Our second aim is to study a bilayer electron system, different from the commonly used symmetrical double square well. Another potentially bilayer electron system is the symmetrical double heterojunction, when the well width is increased a lot, due to the transition from a 'perfect' square quantum well to a system of two separated heterojunctions [20]. In the former structure a high barrier separates the two electron layers. In the latter structure the barrier is formed from the redistribution of the carriers in the well and it is relatively weak. Moreover, Smrčka and Jungwirth [17] have shown, by calculating the energy dispersion curves in a two-subband situation, that symmetrical wide single quantum wells can be potentially bilayer electron systems when the parallel magnetic field is increased. Here, we present the depopulations of the higher subbands and the transition from a single-layer to a bilayer electron system not only in the 'energy dispersion picture', but also in the 'electron concentration picture'. Thus, we calculate the electron concentration, $n(z)$, and the distribution of the electrons in the subbands, $n_i(z)$. We also give the 'density-of-states' picture, which is important for the interpretation of the transport experiments. Moreover, we show in these three pictures that in the centre of our wide quantum well, as the magnetic field is further increased, the bulk Landau levels dominate. Finally, we give an example of an asymmetric heterostructure.

The basic theory is presented in section 2 together with some analogies with the classical picture. In section 3 we present the theoretical results for the $Al_xGa_{1-x}As/GaAs/Al_xGa_{1-x}As$ double heterojunctions and we comment on some interesting features observed. Our conclusions are summarized in section 4.

2. Basic theory

When a magnetic field, $\vec{B}$, parallel to the y-axis, is applied to a three-dimensional electron gas, the motion in the xz-plane is quantized into Landau levels with energy eigenvalues $E_{xz} = \overline{h}\omega(i + \frac{1}{2})$, where i is a discrete quantum number, $\overline{h}$ is the reduced Planck constant and $\omega = eB/m^*$ is the cyclotron frequency. m^* is the effective mass and $q = -e$ is the electron charge. If we additionally apply an electric field, $\vec{E}$, along the z-axis, then E_{xz} depends not

only on i, but also on the wavevector along the x-axis, k_x. Specifically,

$$E_{xz} = \overline{h}\omega\left(i + \frac{1}{2}\right) - \frac{m^*}{2}\left(\frac{E}{B}\right)^2 - \overline{h}k_x\left(\frac{E}{B}\right).$$

In this work we are interested in the configuration with a quantum well along the z-axis (with or without an electric field applied along the z-axis) and the magnetic field applied along the y-axis. Again, as we discuss below, E_{xz} depends on both i and k_x. However, generally in this case $E_{xz} = E_i(k_x)$ cannot be expressed analytically and has to be determined self-consistently. Of course, without a magnetic field, $E_{xz} = E_i + \overline{h}^2k_x^2/(2m^*)$, where now i is the subband index. In all of the situations described above, the y-axis energy eigenvalue is $E_y = \overline{h}^2k_y^2/(2m^*)$, where k_y is the y-axis wavevector. The spin part of the eigenenergy is $E_{spin} = \pm\frac{1}{2}g^*\mu_B B$, where g^* is the effective Landé factor and μ_B is the Bohr magneton.

Summarizing, in the present configuration, there is a magnetic field applied along the y-axis, a quantum well along the z-axis and possibly an electric field applied along the z-axis (e.g. an external field due to a gate). With our choice of axes, the Hamiltonian is

$$\hat{H}_{tot} = (\vec{p} - q\vec{A})^2/(2m^*) + U(z) + g^*\mu_B\vec{\sigma}\cdot\vec{B} \tag{1}$$

where $\vec{p}$ is the momentum operator, $\vec{A}$ is the vector potential, $m^* = 0.067m_e$ is the GaAs effective mass, m_e is the electron mass, $\vec{\sigma}$ is the spin and $\vec{B}$ is the parallel magnetic field. Also,

$$U(z) = U_{band\,offset}(z) + U_C(z) + U_{XC}(z) + U_E(z) \tag{2}$$

where $U_{band\,offset}(z)$ is the potential energy term due to the discontinuities of the conduction band minimum, $U_C(z)$ is the Coulombic potential energy, $U_{XC}(z)$ is the exchange and correlation potential energy [20] and $U_E(z)$ is the potential energy due to an electric field applied in the z-axis direction, e.g. due to a gate. The magnetic field is applied along the y-axis, i.e. $\vec{B} = (0, B, 0)$. For the vector potential we choose $\vec{A} = (Bz, 0, 0)$ [22]. The Hamiltonian becomes

$$\hat{H}_{tot} = (\hat{p}_x - qB\hat{z})^2/(2m^*) + \hat{p}_y^2/(2m^*) + \hat{p}_z^2/(2m^*) + U(z) + g^*\mu_B\vec{\sigma}\cdot\vec{B}. \tag{3}$$

We split the spatial and the spin parts. $\Psi(\vec{r},\vec{\sigma}) = \psi(\vec{r})\alpha(\vec{\sigma})$ and $E_{tot} = E_{xyz} \pm \frac{1}{2}g^*\mu_B B$. For the spatial part the envelope function equation is

$$[(\hat{p}_x - qB\hat{z})^2/(2m^*) + \hat{p}_y^2/(2m^*) + \hat{p}_z^2/(2m^*) + U(z)]\psi = E_{xyz}\psi. \tag{4}$$

$[\hat{p}_x, \hat{H}] = [\hat{p}_y, \hat{H}] = 0$. Thus, we look for solutions in the form $\psi = (1/\sqrt{S})\zeta(z)\mathrm{e}^{\mathrm{i}k_x x}\mathrm{e}^{\mathrm{i}k_y y}$, where $S = L_xL_y$ is the area of the heterostructure in the xy-plane. The coordinate y splits from the coordinates x and z. We have $E_y = \overline{h}^2k_y^2/(2m^*)$, while in the xz-plane

$$\frac{\mathrm{d}^2\zeta(z)}{\mathrm{d}z^2} + \frac{2m^*}{\overline{h}^2}\left[E_{xz} - \frac{m^*}{2}\left(\frac{eB}{m^*}\right)^2\left(z + \frac{\overline{h}k_x}{eB}\right)^2 - U(z)\right]\zeta(z) = 0. \tag{5}$$

The non-magnetic part of the potential energy is $U(z)$, while the magnetic part of the potential energy is

$$\frac{m^*}{2}\left(\frac{eB}{m^*}\right)^2\left(z + \frac{\overline{h}k_x}{eB}\right)^2.$$

The centre of the magnetic potential energy is at the point

$$z_0 = -\frac{\overline{h}k_x}{eB} = -\frac{\overline{h}k_x}{m^*\omega}.$$

Thus, the electron is free in the y-axis direction, but the magnetic field correlates the motion along the x-axis with that along the z-axis. The motion in the xz-plane is characterized by a running wave $\mathrm{e}^{\mathrm{i}k_x x}$ and the bound state $\zeta_{i,k_x}(z)$ which depends on both i and k_x.

The energy eigenvalues are

$$E_{tot} = E_{xz} + E_y \pm \frac{1}{2} g^* \mu_B B = E_i(k_x) + \frac{\overline{h}^2 k_y^2}{2m^*} \pm \frac{1}{2} g^* \mu_B B \tag{6}$$

where, generally, $E_i(k_x) \neq E_i(-k_x)$.

The density of states is

$$n(\mathcal{E}) = \sum_{i,k_x,k_y,\sigma} \delta(\mathcal{E} - E_{i,k_x,k_y,\sigma}) = \sum_{i,k_x} n_{i,k_x}(\mathcal{E}) \tag{7}$$

where

$$n_{i,k_x}(\mathcal{E}) = \sum_{k_y,\sigma} \delta(\mathcal{E} - E_{i,k_x,k_y,\sigma}) = 2 \sum_{k_y} \delta\left(\mathcal{E} - E_{i,k_x} - \frac{\overline{h}^2 k_y^2}{2m^*}\right). \tag{8}$$

We have used the notation $E_{i,k_x} \equiv E_i(k_x)$. Integrating over k_y, equation (8) is

$$n_{i,k_x}(\mathcal{E}) = 2 \frac{L_y \sqrt{2m^*}}{4\pi\overline{h}} \frac{1}{\sqrt{\mathcal{E} - E_{i,k_x}}} \Theta(\mathcal{E} - E_{i,k_x}) \tag{9}$$

where Θ is the step function. We must note here that the DOS is not a step-like function, as it is with zero magnetic field.

The electron concentration is

$$n(\vec{r}) = \sum_{i,k_x} n_{i,k_x}(\vec{r}) \tag{10}$$

where

$$n_{i,k_x}(\vec{r}) = \int_{-\infty}^{+\infty} \mathrm{d}\mathcal{E}\, n_{i,k_x}(\mathcal{E}) f_0(\mathcal{E}) |\psi_{i,k_x}(\vec{r})|^2. \tag{11}$$

$f_0(\mathcal{E})$ is the Fermi–Dirac distribution function and $\psi_{i,k_x}(\vec{r})$ is the three-dimensional envelope function. Thus, at finite temperature, T,

$$n_{i,k_x}(\vec{r}) = 2 \frac{\sqrt{2m^*}}{4\pi\overline{h} L_x} |\zeta_{i,k_x}(z)|^2 \int_0^{+\infty} \mathrm{d}\alpha\, \frac{1}{\sqrt{\alpha}} \left[1 + \exp\left(\frac{\alpha + E_{i,k_x} - \mu(T)}{k_B T}\right)\right]^{-1} \tag{12}$$

where $\mu(T)$ is the chemical potential and k_B is the Boltzmann constant. Using equation (12), equation (10) becomes

$$n(z) = \sum_i n_i(z) = \sum_i \sqrt{\frac{2m^*}{\overline{h}^2}} \frac{1}{(2\pi)^2} \times \int_{-\infty}^{+\infty} \mathrm{d}k_x\, |\zeta_{i,k_x}(z)|^2 \int_0^{+\infty} \mathrm{d}\alpha\, \frac{1}{\sqrt{\alpha}} \left[1 + \exp\left(\frac{\alpha + E_{i,k_x} - \mu(T)}{k_B T}\right)\right]^{-1}. \tag{13}$$

Therefore, the sheet electron concentration is

$$N_s = \sum_i N_i = \sum_i \sqrt{\frac{2m^*}{\overline{h}^2}} \frac{1}{(2\pi)^2} \int_{-\infty}^{+\infty} \mathrm{d}k_x \int_0^{+\infty} \mathrm{d}\alpha\, \frac{1}{\sqrt{\alpha}} \left[1 + \exp\left(\frac{\alpha + E_{i,k_x} - \mu(T)}{k_B T}\right)\right]^{-1}. \tag{14}$$

For a Hamiltonian like that of equation (1), $m^* \vec{v} = \vec{p} - q\vec{A}$ [22], which in our case becomes $m^* \hat{v}_x = \hat{p}_x + eB\hat{z}$, $m^* \hat{v}_y = \hat{p}_y$ and $m^* \hat{v}_z = \hat{p}_z$. Thus, after a little algebra we obtain for the acceleration and the force operators along the x-, y- and z-axes, respectively: $\hat{a}_x = +\omega \hat{v}_z$, $\hat{F}_x = +m^* \omega \hat{v}_z$; $\hat{a}_y = 0$, $\hat{F}_y = 0$; and $\hat{a}_z = -\omega \hat{v}_x - (1/m^*) \partial U(\hat{z})/\partial \hat{z}$, $\hat{F}_z = -m^* \omega \hat{v}_x - \partial U(\hat{z})/\partial \hat{z}$. So, along the y-axis there is no force on the electrons, along

the x-axis there is only the Lorentz force, while along the z-axis there is, in addition to the Lorentz force, the force due to the quantum well confining potential.

When there is no quantum well ($U(z) = 0$) the quantities

$$\hat{z}_0 = -\frac{\hat{p}_x}{eB}$$

which correspond to the z-coordinate of the centre of the classical cyclic orbit and

$$\hat{x}_0 = \frac{\hat{p}_z}{eB} + \hat{x}$$

which corresponds to the x-coordinate of the centre of the classical cyclic orbit are constants of the motion. When $U(z) = 0$, the quantity

$$\hat{r}_c^2 = \frac{(\hat{p}_x + eB\hat{z})^2 + \hat{p}_z^2}{m^{*2}\omega^2}$$

which corresponds to the square of the radius of the classical cyclic orbit is also a constant of the motion. Thus, when $U(z)$ can be ignored, the electrons describe the well-known spiral motion.

The algorithm used to solve the above equations self-consistently is divided into the following steps.

(α') We input an initial guess for the non-magnetic potential energy, $U_{in}(z)$.

(β') We solve the envelope function equation (5) for each i and for each k_x to obtain $\zeta_{i,k_x}(z)$ and E_{i,k_x}. Care should be taken in this step to include all possible i and all possible k_x which contribute to the electron concentration. Thus, we start with many subbands and with a wide range of k_x. This means that equation (5) must be solved *many* times.

(γ') $\mu(T)$ can be calculated from charge neutrality [20, 21], using equation (14).

(δ') Thus, we can calculate, from equation (13), $n(z)$ and $n_i(z)$ and therefore $U_{XC}(z)$ [20].

(ϵ') Now the charge density is known and it is used to solve the Poisson equation numerically [20], to obtain $U_C(z)$. We suppose that $\mathrm{d}U_C/\mathrm{d}z(\text{bulk}) = 0$, because there is no net charge in the bulk material. We take into account the different dielectric constants of GaAs and $Al_xGa_{1-x}As$ [20]. Finally, we choose $U_C(\text{left bulk}) = -U_0$, where U_0 is the value of the discontinuity of the conduction band minimum. $U_{XC}(\text{bulk}) = 0$, because the envelope functions decay into the $Al_xGa_{1-x}As$ barriers. Thus, $U(\text{left bulk}) = 0$. All of the structures are long enough along the z-axis that bulk conditions prevail before the ends of the $Al_xGa_{1-x}As$ barriers are reached.

(ς') The output non-magnetic potential energy, $U_{out}(z)$, can now be calculated from equation (2).

(ζ') If $U_{out}(z)$ is 'very close' to $U_{in}(z)$, we have finished. Otherwise, we mix $U_{out}(z)$ and $U_{in}(z)$ to construct the new $U_{in}(z)$ and we return to step (β') [20].

Finally, we notice that since the envelope functions depend on both i and k_x, a quantitative calculation of the conductivity will involve tedious algebra, because the scattering matrix elements will depend on k_x, too. This complication emerges also in the calculation of the screening. For this reason, although some attempts at obtaining one have already been made [23], a well established transport theory for a Q2DEG with an in-plane magnetic field has not been developed yet.

3. Results and discussion

We apply our treatment to the case of a symmetrical δ-doped $Al_xGa_{1-x}As/GaAs/Al_xGa_{1-x}As$ double heterojunction, in the presence of a parallel magnetic field, ranging from 0 T up to

20 T. We choose a symmetrical structure because in this case we can observe most clearly the variation of the electronic states induced by the magnetic field in the 'energy dispersion picture', in the 'electron concentration picture' and in the 'density-of-states picture'. The structure consists of a 280 Å undoped $Al_{0.25}Ga_{0.75}As$ layer, a Si δ-doped $Al_{0.25}Ga_{0.75}As$ layer (0.28×10^{12} cm^{-2}), an undoped 250 Å $Al_{0.25}Ga_{0.75}As$ spacer, a 600 Å undoped GaAs well, an undoped 250 Å $Al_{0.25}Ga_{0.75}As$ spacer, a Si δ-doped $Al_{0.25}Ga_{0.75}As$ layer (0.28×10^{12} cm^{-2}) and a 280 Å undoped $Al_{0.25}Ga_{0.75}As$ layer. All layers are assumed to have slight unintentional acceptor doping of 1×10^{15} cm^{-3}. We suppose that the sample has been illuminated and that therefore all of the donors are ionized. This is done because we want to study the effect of the magnetic field under the condition of constant sheet electron concentration. Although our treatment is applicable to any temperature, we will apply it to $T = 4.2$ K. This is done because the experiments are usually performed at or below $T = 4.2$ K. These material and structural parameters result in a sheet electron concentration of $N_s = 0.54 \times 10^{12}$ cm^{-2}.

First we will describe the evolution of the changes induced by the magnetic field to the energy dispersion curves, $E_i(k_x)$. The situation is displayed in the lower parts of figure 1. In this particular structure, for $B = 0$, due to the large well width, the ground-state subband and the first and second excited subbands are populated, with sheet electron concentrations of $N_0 = 0.238 \times 10^{12}$ cm^{-2}, $N_1 = 0.233 \times 10^{12}$ cm^{-2} and $N_2 = 0.069 \times 10^{12}$ cm^{-2}, respectively. Initially, as the magnetic field is increased, depopulation of the higher subbands is predicted. The second excited subband is depopulated at $B \simeq 5$ T and the first excited subband at $B \simeq 7$ T. On increasing the magnetic field up to 7 T, the shapes of the $E_i(k_x)$

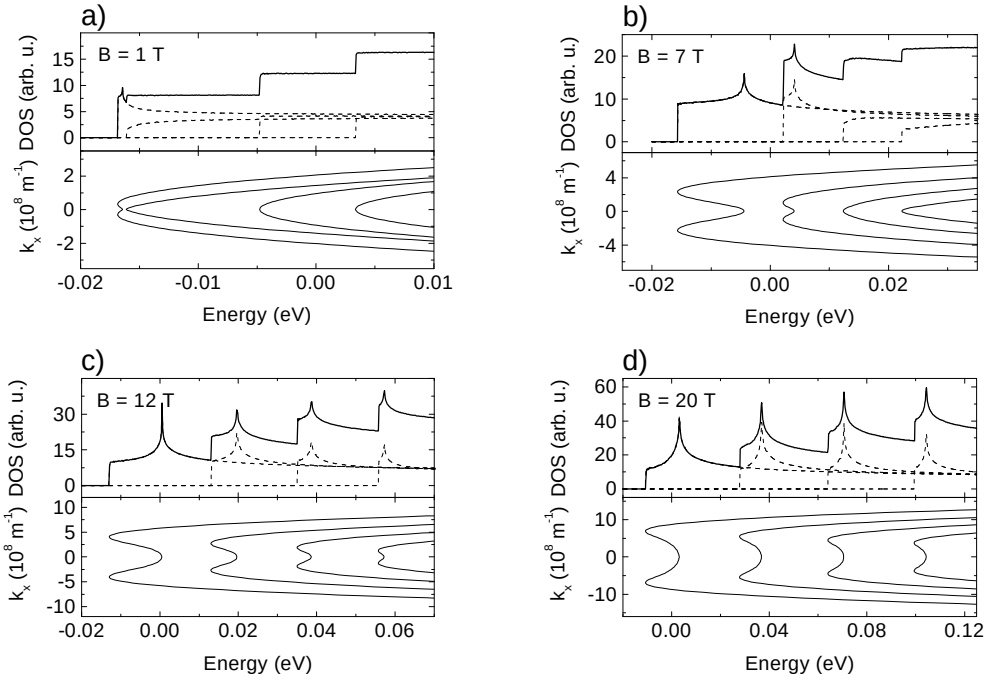

Figure 1. Symmetric heterostructure. The energy dispersion curves, $E_i(k_x)$, $i = 0, 1, 2, 3$ (lower parts), and the densities of states (upper parts) drawn with a common horizontal energy axis for (a) $B = 1$ T, (b) $B = 7$ T, (c) $B = 12$ T and (d) $B = 20$ T. The DOS is in arbitrary units. The chemical potential is identified with the zero energy. The dashed curves represent the DOS of each of the subbands, $n_i(\mathcal{E})$, while the bold continuous curves represent the total DOS, $n(\mathcal{E})$.

dispersion curves also change. While the upper subbands remain almost parabolic, the first excited subband and, most obviously, the ground-state subband undergo important changes, gradually developing local maxima at $k_x = 0$ instead of local minima at $B = 0$ T. As can be seen from the lower parts of figure 1, this also happens to the other excited subbands for larger values of the magnetic field. For $B > 7$ T, only the ground-state subband is populated. At this point the $E_0(k_x)$ dispersion curve is continuously below the chemical potential in the range $k_x = [-4 \times 10^8, +4 \times 10^8]\ \mathrm{m}^{-1}$. This means that the system is still a single-layer one.

At higher magnetic fields, a transition from a single-layer to a bilayer electron system occurs. This transition has approximately been achieved at $B = 12$ T as can be seen from the lower part of figure 1(c), but the complete separation of the two layers is achieved at $B = 20$ T (see figure 2 where the electron concentrations are presented). During this procedure, the energy separation of the unoccupied states (those with small $|k_x|$) becomes $\hbar\omega$. This is due to the fact that the well width is very large and therefore in the central region of the well, as the magnetic confinement overcomes the well confinement, the bulk Landau levels dominate. This has also been predicted for square, analytically solvable, quantum wells when the well width is large enough [16].

In the case of a square quantum well, the behaviour of the $E_i(k_x)$ curves is determined by the competition of the *well width* and the *magnetic length* [16]:

$$l_B = \sqrt{[\hbar/(eB)]}.$$

When the well width is smaller than the magnetic length, spatial quantization dominates. The energy levels can be roughly classified into two types, namely *confined* states and *extended* states. In this *specific case* the confined states in the quantum well increase parabolically as a function of k_x [7, 14], while the extended states have an oscillating form with an 'average' separation of $\hbar\omega$ [7]. However, as the well width or the magnetic field is increased, this behaviour changes. Finally, when the well width is larger than the magnetic length, the electron orbits are governed by the Lorentz force and electrons basically describe spiral motion. At this point the energy dispersion curves are flat with a separation of $\hbar\omega$.

In reference [14], the author, studying thin single quantum wells and taking as the growth axis the z-axis and the magnetic field along the x-axis, bypasses the dependence of the electronic states on the in-plane wavevector along the y-axis (perpendicular to $\vec{B}$), using only $k_y = 0$. This is done in order to reduce the large numerical cost of the general case. It is evident from the lower parts of figure 1 that such an approximation cannot be applied in our case because of the strong dependence of the electronic states on this wavevector. Moreover, for high enough values of the magnetic field, the states with this wavevector are not occupied.

The 'density-of-states picture' is given in the upper parts of figure 1. We observe that although for $B = 1$ T (figure 1(a)) the DOS is almost step-like, there is already a peak due to the fact that $E_0(k_x)$ has already developed a local maximum at $k_x = 0$, instead of the local minimum at $B = 0$ T. This corresponds to a van Hove singularity, since $\mathrm{d}E_0(k_x)/\mathrm{d}k_x > 0$ as we approach the critical point from below and $\mathrm{d}E_0(k_x)/\mathrm{d}k_x < 0$ as we approach the critical point from above. The DOS of the first excited subband is not a 'perfect step', because $E_1(k_x)$ is not exactly parabolic. The densities of states for the second and the third excited subbands are 'perfect steps', because $E_2(k_x)$ and $E_3(k_x)$ are parabolic. We can also see that we have three populated subbands.

In the upper part of figure 1(b) we present the DOS for $B = 7$ T. Clearly, we can observe the depopulation of the first excited subband. Therefore, at this point, as we increase the magnetic field, the conductivity of the structure increases abruptly, due to the abrupt decrease of the DOS at the chemical potential. We also observe that the total DOS is not step-like and that the second and the third excited subbands are not exactly parabolic. Moreover, since

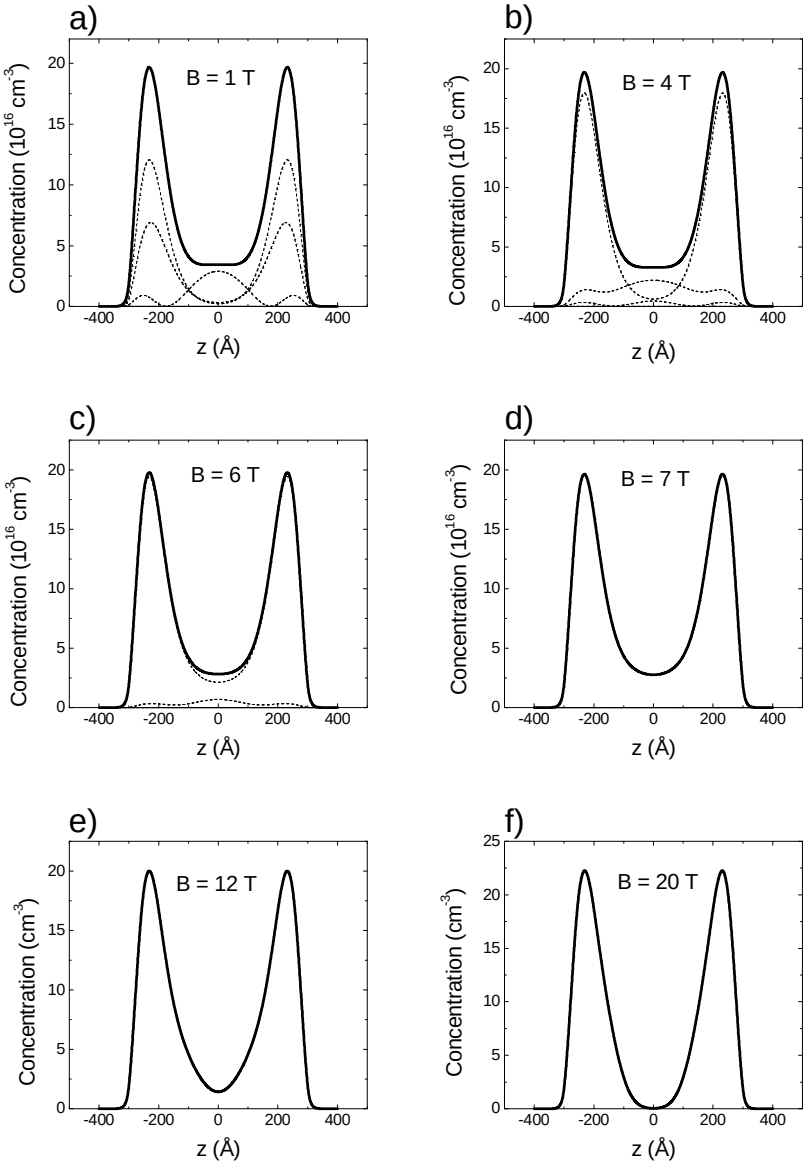

Figure 2. Symmetric heterostructure. The electron concentration, $n(z)$ (bold continuous curves), and the population of the subbands, $n_i(z)$ (dotted curves), for (a) $B = 1$ T, (b) $B = 4$ T, (c) $B = 6$ T, (d) $B = 7$ T, (e) $B = 12$ T and (f) $B = 20$ T.

$E_0(k_x)$ and $E_1(k_x)$ have developed local maxima at $k_x = 0$, there are two peaks in the DOS, corresponding to the two van Hove singularities.

In the upper part of figure 1(c) we present the DOS for $B = 12$ T. There is a van Hove singularity at the chemical potential, due to the local maximum of $E_0(k_x)$ at $k_x = 0$. Therefore, at this point, as we increase the magnetic field, the conductivity of the structure decreases abruptly due to the abrupt increase of the DOS at the chemical potential. The total DOS indicates that at the centre of the well the bulk Landau levels start to develop. All $E_i(k_x)$ have

already developed local maxima at $k_x = 0$ and the energy separation of successive subbands for small $|k_x|$ is close to $\hbar\omega$.

In the upper part of figure 1(d) we present the DOS for $B = 20$ T. The form of the total DOS stems from the combination of two factors, i.e. as we move along the energy axis to higher energies:

(a) From the two local minima of $E_i(k_x)$ up to the local maximum of $E_i(k_x)$ the bilayer electron system dominates.

(b) From the local maximum of $E_i(k_x)$ up to the local minima of $E_{i+1}(k_x)$, the bulk Landau levels dominate. In this region the DOS has the form

$$\text{constant} \times \sum_i \left(\mathcal{E} - \hbar\omega\left(i + \frac{1}{2}\right)\right)^{-1/2} = \text{constant}' \times \sum_{i,k_y} \delta\left(\mathcal{E} - \hbar\omega\left(i + \frac{1}{2}\right) - \frac{\hbar^2 k_y^2}{2m^*}\right)$$

which is the DOS of a free particle on the y-axis together with a harmonic oscillator in the xz-plane. The energy separation of successive subbands for small $|k_x|$ is equal to $\hbar\omega$.

Figure 2 presents the variation of the electron concentration, $n(z)$, and of the population of the subbands, $n_i(z)$, as we increase the magnetic field from 0 T to 20 T. The depopulation of the second excited subband at $B \simeq 5$ T and of the first excited subband at $B \simeq 7$ T can also be seen in this 'electron concentration picture'. Inspection of figure 2 reveals that, in addition to these depopulations, the form of $n(z)$ changes even from 1 T to 7 T, with a slightly bigger separation of the two parts of $n(z)$. This separation increases with the increase of the magnetic field. At 12 T there are still electrons in the middle of the well. The division into two parts is complete at 20 T. This means that the 'electron concentration picture' gives a more precise depiction of the transition to a bilayer system than the 'energy dispersion picture'.

We finally give an example of an asymmetric heterostructure. The structure consists of a 700 Å undoped $Al_{0.25}Ga_{0.75}As$ layer, a 50 Å Si-doped $Al_{0.25}Ga_{0.75}As$ layer (2×10^{18} cm^{-3}), an undoped 50 Å $Al_{0.25}Ga_{0.75}As$ spacer, a 600 Å undoped GaAs well, an undoped 200 Å $Al_{0.25}Ga_{0.75}As$ spacer, a 50 Å Si-doped $Al_{0.25}Ga_{0.75}As$ layer (1×10^{18} cm^{-3}) and a 600 Å undoped $Al_{0.25}Ga_{0.75}As$ layer. We suppose, again, that all of the layers have slight unintentional acceptor doping of 4×10^{14} cm^{-3} and that the sample has been illuminated with the result that all of the donors are ionized. $T = 4.2$ K. These material and structural parameters result in a sheet electron concentration of $N_s = 1.491 \times 10^{12}$ cm^{-2}. For $B = 0$ T, there are four populated subbands with sheet electron concentrations of $N_0 = 0.742 \times 10^{12}$ cm^{-2}, $N_1 = 0.406 \times 10^{12}$ cm^{-2}, $N_2 = 0.229 \times 10^{12}$ cm^{-2} and $N_3 = 0.114 \times 10^{12}$ cm^{-2}, respectively.

In figure 3 we present the energy dispersion curves, $E_i(k_x)$ (lower part), and the densities of states (upper part) for $B = 5$ T. We notice that for this asymmetric heterostructure $E_i(k_x) \neq E_i(-k_x)$. The populations of the subbands are now $N_0 = 1.042 \times 10^{12}$ cm^{-2}, $N_1 = 0.324 \times 10^{12}$ cm^{-2}, $N_2 = 0.110 \times 10^{12}$ cm^{-2} and $N_3 = 0.015 \times 10^{12}$ cm^{-2}, respectively. We can observe the 'transposition and the anticrossings of the parabolas' which result in a complicated form for the DOS. We can also see that there are two different van Hove singularities which give the peaks in the DOS.

Generally, both in the symmetrical and in the asymmetrical case, the van Hove singularities are not simply saddle points, because the $E_i(k_x)$, as we approach the critical points, are not of the form $-\alpha k_x^2$, $\alpha > 0$. The exact form of the dispersion curves is obtained from the self-consistent calculation. Anyway, as we increase the magnetic field, whenever the chemical potential is identified with a van Hove singularity, the conductivity of the structure will decrease abruptly. In contrast, whenever there is a depopulation of a local energy dispersion minimum, due to the decrease of the DOS at the chemical potential, the conductivity will increase abruptly.

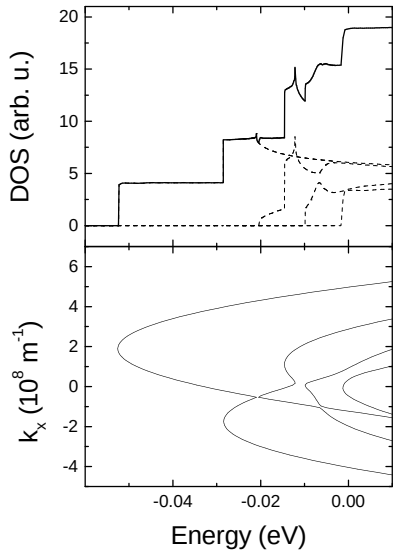

Figure 3. Asymmetric heterostructure. The energy dispersion curves, $E_i(k_x)$, $i = 0, 1, 2, 3$ (lower part), and the densities of states (upper part) drawn with a common horizontal energy axis for $B = 5$ T. The DOS is in arbitrary units. The chemical potential is identified with the zero energy. The dashed curves represent the DOS of each of the subbands $n_i(\mathcal{E})$, while the bold continuous curves represent the total DOS, $n(\mathcal{E})$.

Similar results are obtained for other values of the well width. It is the competition between the magnitude of the magnetic field and the spatial quantization—together with the influence of the number of electrons—that determines the overall behaviour of the system. Extensive comparison with experiment will be presented in a forthcoming paper [24].

4. Summary

Here we have self-consistently calculated the energy dispersion curves, the density of states, the electron concentration and the distribution of the electrons in the subbands for $Al_xGa_{1-x}As/GaAs/Al_xGa_{1-x}As$ double heterojunctions subjected to an in-plane magnetic field.

We have systematically studied the important changes in the density of states, induced by the variation of the in-plane magnetic field. We have pointed out that these changes are of crucial importance for the explanation of the magnetoconductivity experiments.

In the case of symmetric heterostructures, we have demonstrated in the 'energy dispersion picture', in the 'electron concentration picture' and in the 'density-of-states picture' the depopulation of the higher subbands, the transition from a single-layer to a bilayer electron system and the domination of the bulk Landau levels in the centre the wide quantum well, as the magnetic field is continuously increased. We have also given an example of an asymmetric heterostructure.

Acknowledgments

The author wishes to thank Professor Fabio Beltram and Dr Vincenzo Piazza for many useful discussions and for providing the motivation for this work.

References

[1] Fowler A B, Fang F F, Howard W E and Stiles P J 1966 *Phys. Rev. Lett.* **16** 901
[2] von Klitzing K, Dorda G and Pepper M 1980 *Phys. Rev. Lett.* **45** 494
[3] Tsui D C, Störmer H L and Gossard A C 1982 *Phys. Rev. Lett.* **48** 1559
[4] Jungwirth T and Smrčka L 1993 *J. Phys.: Condens. Matter* **5** L217
[5] Heisz J M and Zaremba E 1993 *Semicond. Sci. Technol.* **8** 575
[6] Ohno H and Sakaki H 1982 *Appl. Phys. Lett.* **40** 893
[7] Lee H R, Oh H G, George T F and Um C I 1989 *J. Appl. Phys.* **66** 2442
[8] Gumbs G 1996 *Phys. Rev.* B **54** 11 354
[9] Lyo S K 1994 *Phys. Rev.* B **50** 4965
[10] Simmons J A, Lyo S K, Harff N E and Klem J F 1994 *Phys. Rev. Lett.* **73** 2256
[11] Ohno Y, Sakaki H and Tsuchiya M 1994 *Phys. Rev.* B **49** 11 492
[12] Kurobe A, Castleton I M, Linfield E H, Grimshaw M P, Brown K M, Ritchie D A, Pepper M and Jones G A C 1994 *Phys. Rev.* B **50** 4889
[13] Lay T S, Ying X and Shayegan M 1995 *Phys. Rev.* B **52** R5511
[14] Xu W 1995 *Phys. Rev.* B **51** 9770
[15] Oliveira G M G, Gomes V M S, Chaves A S, Leite J R and Worlock J M 1987 *Phys. Rev.* B **35** 2896
[16] Wang Ch-S and Chuu D-S 1993 *Physica* B **191** 227
[17] Smrčka L and Jungwirth T 1995 *J. Phys.: Condens. Matter* **7** 3721
[18] Jungwirth T, Lay T S, Smrčka L and Shayegan M 1997 *Phys. Rev.* B **56** 1029
[19] Denk P, Hartung M, Streibl M, Wixforth A, Campman K L and Gossard A C 1998 *Phys. Rev.* B **57** 13 094
[20] Simserides C D and Triberis G P 1993 *J. Phys.: Condens. Matter* **5** 6437
[21] Simserides C D and Triberis G P 1995 *J. Phys.: Condens. Matter* **7** 6317
[22] Landau L D and Lifshitz E M 1965 *Quantum Mechanics (Non-Relativistic Theory)* (Oxford: Pergamon) pp 421–7
[23] Tang H and Butcher P N 1988 *J. Phys. C: Solid State Phys.* **21** 3313
Tang H and Butcher P N 1988 *J. Phys. C: Solid State Phys.* **21** 3959
Středa P, Vašek P and Cukr M 1995 *Phys. Rev.* B **51** 11 144
Heisz J M and Zaremba E 1996 *Phys. Rev.* B **53** 13 594
[24] Piazza V, Simserides C D, Wegscheider W and Beltram F, unpublished